



Clinical study

Physiologic characterisation of glioblastoma multiforme using MRI-based hypoxia mapping, chemical shift imaging, perfusion and diffusion maps [☆]

Kathryn M. McMillan ^{a,*}, Baxter P. Rogers ^b, Aaron S. Field ^c, Angela R. Laird ^d, Jason P. Fine ^e, M. Elizabeth Meyerand ^a

^a Department of Medical Physics, University of Wisconsin, Madison, 1530 Medical Sciences Center, 1300 University Avenue, Wisconsin, USA

^b Institute of Imaging Science, Vanderbilt University, Nashville, Tennessee, USA

^c Department of Radiology, University of Wisconsin, Madison, Wisconsin, USA

^d Research Imaging Center, University of Texas Health Science Center, San Antonio, Texas, USA

^e Department of Biostatistics, University of Wisconsin, Madison, Wisconsin, USA

Received 14 June 2005; accepted 1 December 2005

Abstract

Purpose: A multiparametric, physiologic MRI approach was considered to more completely characterise biopsy-confirmed glioblastoma multiforme (GBM). Chemical shift imaging (CSI) supplied biochemical information in metabolite ratios, while perfusion images provided data on presumed vascularity from regional cerebral blood volume (rCBV) and permeability maps. Diffusion-weighted images were reduced to apparent diffusion coefficient (ADC) maps to evaluate cellularity, and blood oxygen level-dependent imaging was used to create maps of putative hypoxic regions.

Methods: Six post-treatment GBM patients were scanned at 3-month intervals until recurrence was suggested by conventional MRI parameters, yielding 20 scans for consideration. The percentage of extreme values in each technique that overlapped with other parameters was measured and compared across hemispheres to assess utility.

Results: We found significantly better performance in selecting the diseased hemisphere for overall percent overlap when compared to voxel counts from individual thresholded parameter maps. Parameters were selected on the basis of highest overlap, and corresponding composite overlap maps show increased specificity to likely recurrent regions by reducing the number of falsely positive voxels, and offer insight into relationships between various parameters.

Conclusion: In a pilot group of patients, percent overlap appears to be sensitive to recurrent disease. When used to combine multiple parameters, voxels containing overlap can specifically target probable recurrent areas.

© 2006 Published by Elsevier Ltd.

Keywords: Glioblastoma multiforme; MRI; Hypoxia; CSI; Diffusion; Perfusion

1. Introduction

Glioblastoma multiforme (GBM) are the most aggressive of primary brain tumours and the outcomes of these

patients have remained unchanged for several decades. Patients are normally treated using a combination of surgery and radiotherapy.¹ Chemotherapy yields limited survival benefit. With these approaches, the overall median survival is approximately 50 weeks.² Since therapy is not optimal, patients are likely to relapse after initial treatment. Following patients after completion of surgery and radiation therapy could allow for a greater understanding of recurrent disease as well as allowing for earlier and more effective treatment options. Increased understanding of the tumour

[☆] This work was presented as posters at the ISMRM 11th and 12th annual meetings, 2003–2004. Grant information NIH R01 EB00448-02 NIH 1F31NS046168-01A1.

* Corresponding author. Tel.: +608 263 0066; fax: +608 265 9840.

E-mail address: kathryn.mcmillan@vanderbilt.edu (K.M. McMillan).

environment via imaging modalities offers an opportunity for neurosurgeons to collect samples and validate techniques. These parameter maps may also give increased insight into tumour extent as treatment effects can cause ambiguity on T1- and T2-weighted images (see Fig. 1).

Patients with GBM most often have a heterogeneous, irregular, contrast-enhancing lesion seen on MRI that shows infiltration into surrounding brain, often believed to be described by the T2-weighted MRI signal abnormality. T1-weighted MRI with the use of a contrast agent usually underestimates tumour volumes, as contrast enhancement is more a reflection of blood-brain barrier breakdown than actual tumour extent. Disruption of the blood-brain barrier through treatment confounds the images acquired to monitor patients post-radiation therapy. Conversely, T2-weighted images tend to overestimate tumour volumes due to the high signal intensity resulting from surrounding oedema as well as microscopic tumour extension.³ Radiation effects can also mimic microscopic tumour extension, and necrotic areas exist within the heterogeneous environment. Since diagnosis and planning for treatment utilise MR methods, increased information describing tumour extent and functional regions within the heterogeneous environment would be useful.

Extensive data have been collected on chemical shift imaging (CSI),^{4–8} perfusion^{3,5,7,9,10} and diffusion imaging,^{5,6,10} as well as MR-based hypoxia mapping that seem to indicate that each of these techniques adds information regarding tumour composition as well as extent.^{11–15} Studies have demonstrated changes in the ratio of metabolites associated with tumour presence using CSI.⁴ Tumour regions displaying increased regional cerebral blood volume (rCBV) or permeability may have either co-opted existing blood vessels to provide support for the rapidly expanding tumour or formed new vasculature.^{3,10} Extracellular space decreases where cells are multiplying quickly, which creates an area where water motion is restricted outside the cells as well as in the more viscous intracellular space. Therefore, low apparent diffusion coefficient (ADC) values are believed to indicate high cellularity.¹⁶ In addition, MR-based hypoxia mapping is thought to delineate oxygen-starved

cells that resist radiation therapy.¹¹ To our knowledge, hypoxia maps have not been combined with spectroscopy, perfusion and diffusion results to characterise GBM.

Finding a more effective treatment option for GBM patients is critical.¹ Yang et al. have shown the value of combining multi-voxel MR spectroscopy, perfusion, and diffusion-weighted images to predict the grade of cerebral gliomas.⁵ In addition, investigations of brain tumour physiology have been performed by combining diffusion imaging with CSI as well as perfusion with CSI.^{6,7} To consider the patients presented here, we used a multiparametric approach to assess the utility of analysing multiple sets of data believed to be predictive of tumour metabolism, proliferative potential, cellularity, and oxygenation status, which we obtained via CSI, perfusion, diffusion and hypoxia scans.

A single map combining information from all relevant techniques is desirable. It is likely that not all parameters will be useful in every patient or at every time-point. We hypothesise that voxels likely to represent recurrent disease will contain information indicative of abnormality from more than one technique. Therefore, we considered overlap among multiple techniques in both hemispheres of six recurrent GBM patients. If the percentage of voxels that participate in overlap with other parameters can be used to select parameters that map regions likely to recur, higher values of overlap should be found in the diseased hemisphere relative to the healthy hemisphere. For comparison purposes, the total number of abnormal voxels reported by each technique was compared across hemispheres. Once particular parameters were selected from the highest overlap percentages, composite maps of tumour areas should show likely recurrent regions located near the original tumour sites.

2. Materials and methods

The study is an Institutional Review Board approved clinical protocol, and all subjects signed informed consent. MR scanning was performed on a clinical 1.5T GE Signa Horizon magnet (GE Medical Systems, Milwaukee, WI,

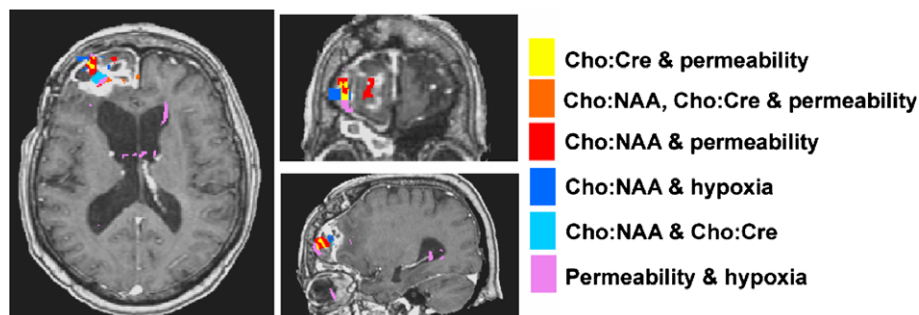


Fig. 1. Representative composite overlap map. Permeability is thought to be a biomarker for immature, leaky vasculature. Correlations with areas of high cell turnover as measured by choline, and areas of hypoxia are seen. Cho:NAA showed 100% overlap; Cho:Cre, 93%; permeability, 19%; hypoxia, 91%. This map gives insight into the recurrent portion of the larger enhancing lesion seen on T1-weighted images. Cho = choline, Cre = creatine, NAA = N-acetyl aspartate.

USA) equipped with gradients for whole-body echo-planar imaging (EPI). To attain optimal registration and minimise motion within a single scan session, the head was immobilised with straps and foam padding before the first scan was acquired. Images were registered by aligning common neuroanatomic landmarks using Analysis of Functional Neuroimages (AFNI) software (National Institute of Mental Health, Bethesda, MD, USA).¹⁷ Acquiring images from the whole-brain volume for perfusion, diffusion and hypoxia data gave an increased number of landmarks resulting in a more exact registration.

Six patients successfully completed all physiologic scanning in addition to conventional techniques. By considering voxels that contain extreme values in more than one technique, we are able to isolate regions where surgical therapy is necessary while offering information regarding the extent and environment of the disease.

2.1. Chemical shift imaging protocol

The scan parameters for the CSI acquisition were TR = 1.0 s, TE = 144 ms, $\theta = 90^\circ$, volume matrix = 8×18 . Post-processing consisted of compensation for residual eddy currents, Gaussian line broadening (time constant, 256 ms), and zero- and first-order phase correction after two-dimensional Fourier transformation. For each voxel, spectroscopic analysis was used to establish the relative amplitudes of peaks corresponding to N-acetyl aspartate (NAA), choline, creatine, and lactate. Metabolic images were formed from the real parts of the spectra after phase and baseline corrections by integration of the signal within the spectral area of the particular metabolite. Three ratio maps (choline:NAA, choline:creatine and lactate:creatine) were formed for percent overlap consideration.

2.2. Perfusion imaging protocol

Perfusion-weighted images were acquired in the axial plane using the acquisition parameters TR = 2 s, TE = 60 ms, $\theta = 60^\circ$, FOV = 22 cm, slice = 7 mm, gap = 2 mm, matrix = 128×128 . Contrast of 0.1 mmol/kg of body weight of a gadodiamide (Omniscan, Nycomed-Amersham, Princeton, NJ, USA) was injected at 4.0 mL/sec followed by a saline flush using a power injector (Spectris, MED-RAD, Indianola, PA, USA) 13 seconds after scan initiation.

We created maps of rCBV using a bolus method. The arterial input function (AIF) was automatically detected based on a standard deviation threshold of signal change. The area under the AIF is used to normalise the tissue curve such that:

$$\text{rCBV} = k/\rho * \int (C_{\text{tissue}}(t)dt) / \int (C_{\text{AIF}}(t)dt) \quad (1)$$

where k/ρ are physiological constants that depend on the blood hematocrit and brain tissue density, C_{tissue} is the gad-

olinium concentration in tissue and C_{AIF} is the gadolinium concentration in the AIF.

Li's first pass leakage profile method was used to calculate permeability maps using

$$C_t(t) = K_{\text{FP}} \int C_p(t')dt' + v_p C_p(t) \quad (2)$$

where C_t is the time course curve of the contrast agent concentration, K_{FP} is the volume transfer constant between the plasma and extracellular extravascular space as calculated from the first pass model, C_p is the tracer concentration in arterial blood plasma, v_p is the volume of blood plasma per tissue unit volume.¹⁸

2.3. Diffusion protocol

Diffusion EPI images were acquired with the parameters as follows: TR = 5 s, TE = 86 ms, $\theta = 90^\circ$, FOV = 22 cm, slice = 5 mm, gap = 0 mm, matrix = 256×256 . Images were obtained at five different b values in each of three orthogonal directions. Diffusion-weighted images were reduced to ADC maps for comparison across patients.¹⁶

2.4. Hypoxia mapping protocol

For the blood oxygen level-dependent MRI (BOLD MRI) (hypoxia mapping), a multi-echo EPI sequence was employed with 10 different echo times (TE) to quantify T_2^* . Parameters were as follows: TR = 1.2 s, TE = 35–80 ms (steps of 5 ms), $\theta = 90^\circ$, FOV = 22 cm, slice = 5 mm, gap = 1 mm, matrix = 128×128 . The patient breathed carbogen (95% O₂, 5% CO₂) through a tube placed in the mouth in order to increase oxygenation in hypoxic areas.¹¹ No patients reported discomfort while breathing this gas mixture, and nose clips were used in later patient scans to ensure carbogen breathing.

Differences between air and carbogen scans are specific to hypoxic areas since oxygenation levels will remain unchanged in normal tissue as well as necrotic areas.^{12,13} During the air-breathing interval, the tube was not attached to the patient, allowing room air breathing. The tube then connected the patient to the carbogen tank and the gas flow was adjusted to a rate of 20 L/min for the equilibration and carbogen breathing intervals. The patient was instructed to breathe only through the mouth at those times. EPI images were initially acquired with normal air breathing. The patient then breathed carbogen gas for a 15-minute equilibration period before the next EPI scan began. The patient continued to breathe the carbogen gas during the acquisition of the second set of multi-echo EPI images.

T_2^* was calculated for air and carbogen breathing by fitting the signal intensity (SI) versus echo time (TE) to a single exponential function using Matlab (Mathworks Corp., Natick, MA, USA) according to the equation:

$$\ln[SI(1)] = -\frac{1}{T_2^*}(TE) + \ln[SI(0)] \quad (3)$$

where $SI(0)$ and $SI(1)$ are the signal intensities at time 0 and 1 respectively. Relative changes between air and carbogen breathing were evaluated using a paired Student's t -test.

2.5. Percent overlap and composite maps

Each physiologic dataset was resampled and aligned to the high-resolution anatomical that was chosen to underlay the composite map, resulting in 1 mm^3 voxels for each technique. The non-tumour hemisphere was used to find appropriate thresholds for each whole-brain parameter map such that suprathreshold voxels would consist of the extreme 5% or 2% of overall values. Each map was then thresholded to contain only the extreme values (high choline:NAA, choline:creatine, lactate:creatine, high rCBV, high permeability, low ADC, and highly significant $T2^*$ differences for hypoxia). When CSI data was not acquired in both hemispheres, the tumour hemisphere was used to obtain the maximum values of the ratio maps. Since optimal threshold percentages were unknown, 5% and 2% were chosen to define extreme values to select moderately and strictly high values, yielding two complete sets of thresholded parameter maps. Each thresholded map contains a certain number of voxels, called voxels_x , where x is the individual parameter (e.g. ADC, rCBV, hypoxia).

A single map containing all seven parameters was formed where the intensity indicated which parameters that overlapped in each voxel. Zeros were assigned to voxels that did not contain extreme values for any technique. Unique values were then assigned to each of the seven thresholded parameter maps and sums were calculated. A unique value then existed for every possible combination of techniques. Assigning unique values allowed for the determination of which parameters overlapped in each voxel so the maps could be colour-coded. Voxels for each value were then counted. Percent overlap was calculated for each technique x , using

$$\text{Percent overlap} = (\text{voxels}_x - \text{voxels}_{\text{only}x}) / \text{voxels}_x \quad (4)$$

where voxels_x was defined previously as the total number of voxels in a thresholded parameter map, and $\text{voxels}_{\text{only}x}$ counts the voxels for technique x that do not show overlap with any other technique. Therefore, the numerator gives the number of voxels that overlap with any other technique and the denominator counts every voxel in the thresholded map regardless of overlap. Calculations were performed for each hemisphere separately in each parameter.

A parameter was considered successful if the disease hemisphere showed increased overlap or total voxels compared to the contralateral hemisphere. Total voxels were compared to percent overlap measures for each technique separately and for all techniques combined to determine differences using McNemar's test. Comparisons of performance at different thresholds were also performed by comparing percent overlap using the extreme 2% of values and 5% of values. A similar examination was performed for the total number of voxels at the two threshold levels.

Voxels containing larger numbers of overlapping component techniques are more compelling. For example, if all seven techniques indicate a given voxel is abnormal, we would be very confident that the physiology in that area was truly of interest. Overlap percentages were therefore weighted according to the number of techniques that overlapped in a given voxel (i.e. voxels containing two overlapping techniques were weighted by 1, three techniques by 2).

After examination of overlap values and selection of likely relevant techniques with highest percent overlap, physiologic composite maps were formed in AFNI. The top four overlap values were chosen unless a given overlap percentage was less than or equal to the contralateral value. In some cases, fewer parameters were selected if the disease hemisphere did not exceed the amount of overlap in the healthy hemisphere for multiple parameters. Voxels containing overlap are displayed as functional overlays with corresponding colour bars.

3. Results

Total suprathreshold voxels per technique were considered along with percent overlap for 20 scans. Parameter performance was judged individually at both threshold levels separately, and the performance of percent overlap in selecting the diseased hemisphere was compared to that of voxel number in thresholded parameter maps. Results in Table 1 are given for each parameter, and show the percent of 20 scans having greater value in the diseased hemisphere. It is critical to observe that of the 20 available scans, only four of these truly represent recurrent cancer processes. The majority are acquired at stable time-points and show little, if any, evidence of physiologic processes of interest. The performance of overlap maps was not significantly different than voxel counts from individually thresholded maps ($p < 0.05$) for most parameters. However, rCBV performance was significantly greater using overlap maps at the 5% threshold ($p = 0.016$), while hypoxia overlap percentage was greater than the number of vox-

Table 1
Percentage of parameter maps that had higher measures (number of voxels or percentage overlap) in the diseased hemisphere

	Overlap ₅ %	Voxels ₅	Overlap ₂ %	Voxels ₂
ADC	100	78%	78	78%
rCBV	89	55%	89	44%
Hypoxia	100	55%	100	44%
Permeability	78	100%	100	89%
Cho:NAA	89	78%	78	78%
Cho:Cre	100	89%	100	78%
Lac:Cre	100	100%	89	89%
Overall	94	82%	92	75%

While the disease hemisphere does not always contain more voxels, higher overlap percentages are consistently found in the tumour hemisphere. The comparison across hemispheres offers a method for selecting the most relevant parameters.

ADC = apparent diffusion coefficient, rCBV = regional cerebral blood volume, Cho = choline, NAA = N-acetyl aspartate, Cre = creatine, Lac = lactate.

els for both percentages, $p = 0.03$ at 5%, and $p = 0.016$ at 2%.

To increase sample size, values were compared by condensing the seven parameter values to a single overall percentage. Statistically significant differences were found when comparing percent overlap to the total voxels using 5% threshold (94% vs. 79%), p -value <0.001 , and a 2% threshold (94% vs. 81%), p -value <0.001 . Neither the differences between 5% overlap and 2% overlap, 5% total voxels versus 2% total voxels were statistically significant using the McNemar's test for individual parameters or overall measures.

A representative patient map is shown for reference, and the composite map was created using the 5% threshold values (Fig. 1). Permeability, hypoxia, Cho:NAA and Cho:Cre were the most relevant parameters for the recurrent time-point for this patient. Areas of overlap are seen in the central portion of the enhancing areas. Hypoxia and permeability overlap in ventricle areas, likely reflecting blood flow effects from each technique. When considering hypoxia and permeability maps alone, however, many additional areas would need to be examined for lack of specificity. The overlap map clearly decreases the appearance of areas not corresponding to tumour processes.

4. Discussion

Multiple techniques have been found to correlate with each other and there have been many studies that indicate MR parameters give insight into tumour physiology.^{5–7,19} However, recent comparisons show some lack of reliability in using individual techniques as well as new trends when combining parameters.^{19,20} As increasing numbers of biomarkers are developed for MRI, it is increasingly important to determine which techniques are most significant in a patient at a particular time. In addition to evaluation against gold standards, determination of how these techniques relate to each other is relevant.

Primary brain tumours are likely to be confined to a single hemisphere, and often will recur within a few cm of the resection bed.¹ Since physiologic parameters may change over time through various treatment modalities and recovery processes, normalising tumour tissue to contralateral healthy tissue could provide an important measure of abnormality. If a method reflects physiology related to tumour cells, the measures obtained in the diseased hemisphere should be greater than those found in contralateral brain tissue. While using multiple techniques clearly offers advantages in finding complementary regions showing separate physiologic processes, our focus on redundant areas allows reduction of false positives that exist in the individual thresholded parameter maps.

Some voxels will overlap by chance when forming a composite map of any combination of parameters. By performing whole-brain calculations and considering the hemispheres separately, the healthy hemisphere can be used to estimate the number of overlaps that occur by chance.

This provides an estimate of false positives that occur for that patient and for the specific combination of parameter maps chosen. If the diseased hemisphere does not result in greater overlap percentages for a parameter, it is considered to represent noise and not relevant tumour information at that time-point. Depending on the physiologic processes, not all techniques will yield useful information at every time-point. By comparing results to the values in the healthy hemisphere and estimating noise, the worth of each parameter map can be evaluated.

Six to eight percent of overlap values were higher in the healthy hemisphere depending on the threshold value utilised. In those cases, the differences between hemisphere values tended to be small. In contrast, the number of voxels above the threshold in each technique yielded a greater value in the healthy hemisphere 18–25% of the time. Therefore, we maintain that percent overlap could be a relevant way to consider multiple physiologic techniques for further consideration in hopes of forming a single descriptive map.

In forming composite maps, whole brain techniques were used for most parameters. By considering all values, rather than placing a subjective region of interest, a good estimation of noise was achieved and maps were subjectively unbiased toward tumour areas in perfusion, diffusion and hypoxia maps. CSI data were sometimes acquired in a smaller region placed in the most abnormally-appearing areas to achieve optimal shimming. So while we have taken care not to introduce additional subjective regions of interest into the percent overlap, some initial bias is in place and could account for some of the specificity to the tumour site. CSI overlaps with many techniques and at least one ratio map has been included in all images.^{5–7} When possible, larger PRESS (Point RESolved Spectroscopy) boxes should be utilised to include contralateral tissue to obtain estimates of noise in the healthy hemisphere. CSI is a valuable parameter due largely to the high specificity to the tumour region. By using this advantage in overlap calculations, composite maps of multiple techniques show similar specificity.

Additional subjectivity is introduced when choosing a value for thresholding each map. When comparing the total number of voxels and overlap percentages for both 2% and 5% thresholds, no significant differences were found when considering individual parameters or condensed overall measures. Using a more moderate threshold of 5% may have value. Moderate increases in the percentage of values greater in the diseased hemisphere were found for both percent overlap and total voxel counts. From our dataset, it appears that the technique is relatively insensitive to thresholding percentage for parameter selection purposes.

When many parameters are considered for recurrent patients, the amount of information can become overwhelming and therefore of limited use. Combining multiple parameters in an easy to read map is therefore desirable for use in surgical planning when tremendous radiological

information must be condensed to the key factors. By finding the most appropriate techniques at every time-point, the number of parameters of interest can be reduced in a standard way. These parameters of interest can then be considered by knowledge-based techniques, clustering algorithms, nosologic images or in composite overlap maps.^{21–23} The latter considers only voxels with multiple techniques that show overlap in hopes of highlighting regions of interest. Composite maps in the patient presented here are highly specific to tumour areas.

Surveys of three radiologists were completed on the individual parameter maps, and the percent overlap technique always selected the same parameters as the radiological consensus. The exception was that hypoxia was often selected by the overlap technique as being relevant at recurrent time-points, while radiologists seldom selected the technique as corroborating their initial diagnosis. The role of BOLD-based hypoxia imaging is therefore greater in an automated technique when compared to radiology opinions.

In addition, improved modelling of the complex tumour physiology is ongoing. All of the parameters used here will likely increase in quality as human and animal research evolves. We obtained clinically relevant information to monitor patients post-treatment. When considering the information offered by these scans, the composite maps of the most relevant parameters offer a great deal of insight into the most dangerous functional regions of the tumour recurrence.

Since a majority of patients relapse locally, we expected to see voxels highlighted in composite maps located close to the resection bed.²⁴ A 60-year-old woman completed radiotherapy after surgery confirmed an initial high grade glioma. Recurring 2 years after the completion of external beam radiation therapy, she was treated with stereotactic radiosurgery. Follow-up examinations with physiologic parameters were obtained 4 and 7 months post-surgery. The composite map shown was acquired at the later time-point, and shows physiology indicative of recurrence. While conventional images showed nodular enhancement and a thickening of the enhancing border, additional insight is offered by spectroscopy, perfusion and hypoxia maps.

Permeability is thought to be a measure of angiogenesis, induced by hypoxic environments. High choline, normalised to creatine and NAA, is found near these regions overlapping with hypoxia and permeability. These fast-growing areas could be outgrowing their blood supplies and creating hypoxic conditions where anaerobic metabolism is necessary. These conditions promote angiogenic growth factors, leading to increases in permeability. An overlapping area of hypoxia and increased permeability is located near the hypoxia and choline regions, possibly relating to leaky neovasculature promoted by hypoxic conditions.²⁵ Tumour blood vessels are highly irregular, have arteriovenous shunts and blind ends, and lack normal smooth muscle; as a result, tumour blood flow is highly

variable.³ Since BOLD-based hypoxia mapping has not been used extensively in humans, overlap with relevant techniques provides some support for its utility. Insight into complex physiologic factors is gained for this representative patient.

Subsequent surgery was performed and GBM recurrence has histologically been confirmed. The most medial portion of the tumour was not resected, and a fourth recurrence was later diagnosed in the medial posterior aspect of the right superior frontal gyrus. Both choline ratio maps overlap with permeability measures along the medial portion of enhancement in orange and indicate that these regions are metabolically active and angiogenic. With further validation and better parameter maps, we hope to offer neurosurgeons even higher quality composite maps so that the entire tumour region can be visualised and more optimal treatment delivered.

Since MR parameters are thought to correspond to related physiologic processes, multiple MR techniques should overlap in regions most likely to show tumour growth. By considering the percentage of voxels in a particular parameter that overlap with other parameters, relevant maps can be selected for further consideration and dangerous regions could be more accurately identified on composite maps.

5. Conclusion

As increasing MR parameters become available, it becomes increasingly important to monitor their behavior in relation to one another. Using percent overlap in conjunction with composite maps can offer insight into the extent, environment and possible recurrence regions in GBM patients. As increasing techniques monitor metabolic activity, perfusion characteristics, cellularity and hypoxia in different ways, methods of selecting highly relevant techniques will become increasingly important. Percent overlap appears to offer an effective way to choose valuable parameters from multiple options, and careful consideration of composite maps may aid in the planning of treatment for recurrent patients.

References

1. Hochberg FH, Pruitt A. Assumptions in the radiotherapy of glioblastoma. *Neurology* 1980;**30**:907–11.
2. Stewart LA. Chemotherapy in adult high-grade glioma: a systematic review and meta-analysis of individual patient data from 12 randomised trials. *Lancet* 2002;**359**:1011–8.
3. Knopp EA, Cha S, Johnson G, et al. Glial neoplasms: Dynamic contrast-enhanced T2*-weighted MR imaging. *Radiology* 1999;**211**:791–8.
4. Tedeschi G, Lundbom N, Raman R, et al. Increased choline signal coinciding with malignant degeneration of cerebral gliomas: a serial proton magnetic resonance spectroscopy imaging study. *J Neurosurg* 1997;**87**:516–24.
5. Yang D, Korogi Y, Sugahara T, et al. Cerebral gliomas: prospective comparison of multivoxel 2D chemical-shift imaging proton MR spectroscopy, echoplanar perfusion and diffusion-weighted MRI. *Neuroradiology* 2002;**44**:656–66.

6. Gupta RK, Sinha U, Cloughesy TF, et al. Inverse correlation between choline magnetic resonance spectroscopy signal intensity and the apparent diffusion coefficient in human glioma. *Magn Reson Med* 1999;**41**:2–7.
7. Henry RG, Vigneron DB, Fischbein NJ, et al. Comparison of relative cerebral blood volume and proton spectroscopy in patients with treated gliomas. *Am J Neurorad* 2000;**21**:357–66.
8. Shih MT, Singh AK, Wang AM, et al. Brain lesions with elevated lactic acid peaks on magnetic resonance spectroscopy. *Curr Probl Diagn Radiol* 2004;**33**:85–95.
9. Aronen HJ, Gazit IE, Louis DN, et al. Cerebral blood volume maps of gliomas: comparison with tumor grade and histologic findings. *Radiology* 1994;**191**:41–51.
10. Provenzale JM, Wang GR, Brenner T, et al. Comparison of Permeability in high-grade and low-grade brain tumors using dynamic susceptibility contrast MR imaging. *Am J Roentgenology* 2002;**178**:711–6.
11. Griffiths JR, Taylor NJ, Howe FA, et al. The response of human tumors to carbogen breathing, monitored by gradient-recalled echo magnetic resonance imaging. *Int J Radiat Oncol Biol Phys* 1997;**39**:697–701.
12. Robinson SP, Rodrigues LM, Ojugo AS, et al. The response to carbogen breathing in experimental tumor models monitored by gradient-recalled echo magnetic resonance imaging. *Br J Cancer* 1997;**75**:1000–6.
13. Collingridge DR, Piepmeier JM, Rockwell S, et al. Polarographic measurements of oxygen tension in human glioma and surrounding peritumoural brain tissue. *Radiother Oncol* 1999;**53**:127–31.
14. Dunn JF, O'Hara JA, Zaim-Wadghiri Y, et al. Changes in oxygenation of intracranial tumors with carbogen: a BOLD MRI and EPR oximetry study. *J Magn Reson Imaging* 2002;**16**:511–21.
15. Brown JM. The hypoxic cell: a target for selective cancer therapy. *Cancer Res* 1999;**59**:5863–70.
16. Sugahara T, Korogi T, Kochi M, et al. Usefulness of diffusion-weighted MRI with echo-planar techniques in the evaluation of cellularity in gliomas. *J Magn Reson Imag* 1999;**9**:53–60.
17. Cox RW. AFNI: Software for analysis and visualization of functional magnetic resonance neuroimages. *Comp Biomed Res* 1996;**29**:162–73.
18. Li KL, Zhu XP, Waterton J, et al. Improved 3D quantitative mapping of blood volume and endothelial permeability in brain tumors. *J Magn Reson Imaging* 2000;**12**:347–57.
19. Law M, Yang S, Babb JS, et al. Comparison of cerebral blood volume and vascular permeability from dynamic susceptibility contrast-enhanced perfusion MR imaging with glioma grade. *AJNR Am J Neuroradiol* 2004;**25**:746–55.
20. Pauleit D, Langen KJ, Floeth F, et al. Can the apparent diffusion coefficient be used as a non-invasive parameter to distinguish tumor tissue from peritumoural tissue in cerebral gliomas? *J Magn Reson Imaging* 2004;**20**:758–64.
21. Clark MC, Hall LO, Goldgof DB, et al. Automatic tumor segmentation using knowledge-based techniques. *IEEE Trans Med Imaging* 1998;**17**:187–201.
22. Soltanian-Zadeh H, Pasnoor M, Hammoud R, et al. MRI tissue characterization of experimental cerebral ischemia in rat. *J Magn Reson Imaging* 2003;**17**:398–409.
23. De Edelenyi FS, Rubin C, Esteve F, et al. A new approach for analyzing proton magnetic resonance spectroscopic images of brain tumors: nosologic images. *Nat Am* 2000:1287–9.
24. Wallner KE, Galicich JH, Krol G, et al. Patterns of failure following treatment for glioblastoma multiforme and anaplastic astrocytoma. *International J Radiat Oncol Biol Phys* 1989;**40**:1141–9.
25. Kostourou V, Troy H, Murray JF, et al. Overexpression of dimethylarginine dimethylaminohydrolase enhances tumor hypoxia: an insight into the relationship of hypoxia and angiogenesis in vivo. *Neuroplasia* 2004;**6**:401–11.